

Comparison of Spectral Index Determinations

Edward L. Wright
UCLA Dept. of Astronomy
Los Angeles CA 90024-1562

ABSTRACT

The index n of a power law power spectrum of primordial density fluctuations, $P(k) \propto k^n$, has been estimated using many different techniques. The most precise compare the *COBE*¹ DMR large angular scale ΔT to the amplitude of the large scale structure, but these are also the most model-dependent. The *COBE* DMR ΔT has also been compared to the degree-scale ΔT from several experiments. And finally, a relatively model-independent value of n can be derived from the *COBE* data alone, but the small range of angular scales covered by *COBE* limits the precision of these methods.

1. Introduction

In this paper I compare several different methods for determining the spectral index n of the power spectrum of primordial density perturbations. All of the determinations that use *COBE* data are statistically compatible with the $n \approx 1$ predicted by the inflationary scenario. Because the largest scales appear as large angular scale features on the finite solid angle of sky that is available for viewing, the statistical uncertainties in the determination of n cannot be conquered by the usual expedient of getting more data. A careful consideration of the statistical methods used to analyze the large-angular scale *COBE* data is needed.

2. Biased Statistics

As an example of the pitfalls of statistical analysis, consider the maximum likelihood method applied to determining the standard deviation of a Gaussian from a set of N independent samples drawn from the distribution. The likelihood function is

$$L(\mu, \sigma) = (\sqrt{2\pi}\sigma)^{-N} \prod_{i=1}^N \exp[-0.5(x_i - \mu)^2/\sigma^2] \quad (1)$$

which is maximized at $\mu = N^{-1} \sum_i x_i$ and $\sigma^2 = N^{-1} \sum_i (x_i - \mu)^2$. While the sample mean is an unbiased estimate of the population mean, the variance estimate is biased by a factor of

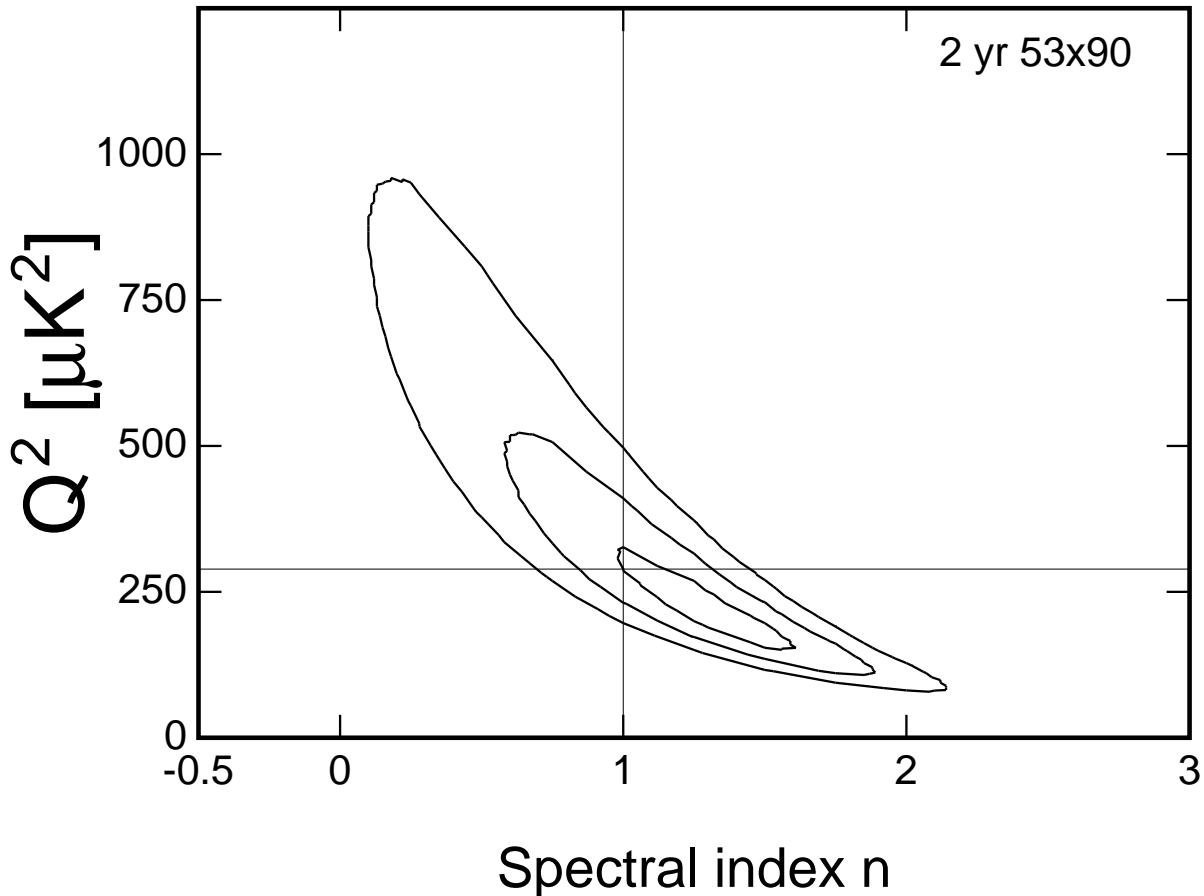


Fig. 1.— Likelihood contours vs Q^2 and n , based on the 2 year 53×90 cross power spectrum for $3 \leq \ell \leq 30$.

$(N - 1)/N$, illustrating the fact that maximum likelihood estimators are only *asymptotically* unbiased. Even with an unbiased estimate of σ , the logarithm of an unbiased estimate of σ is not an unbiased estimate of the logarithm of σ because noise rectification by the second derivative of the logarithm leads to a bias of $-1/4N$. Since the value of N when estimating the power in the ℓ 'th multipole is $N \approx (2\ell + 1)\Omega_{obs}/4\pi$, and since Ω_{obs} is $< 8\pi/3$ due to galactic contamination, these biases will be most significant for the low ℓ 's measured by *COBE*. Thus any method for determining n using *COBE* data should be tested using simulated data to calibrate these biases.

One non-recommended technique for determining n is to treat the integrated likelihood $f(n) = \int L(Q, n)dQ$ as a probability density for n . The usual justification for this is the Bayesian rule that the probability density for Q and n after the experiment, $p_a(Q, n)$, is given by

$$p_a(Q, n) \propto p_p(Q, n)L(Q, n) \quad (2)$$

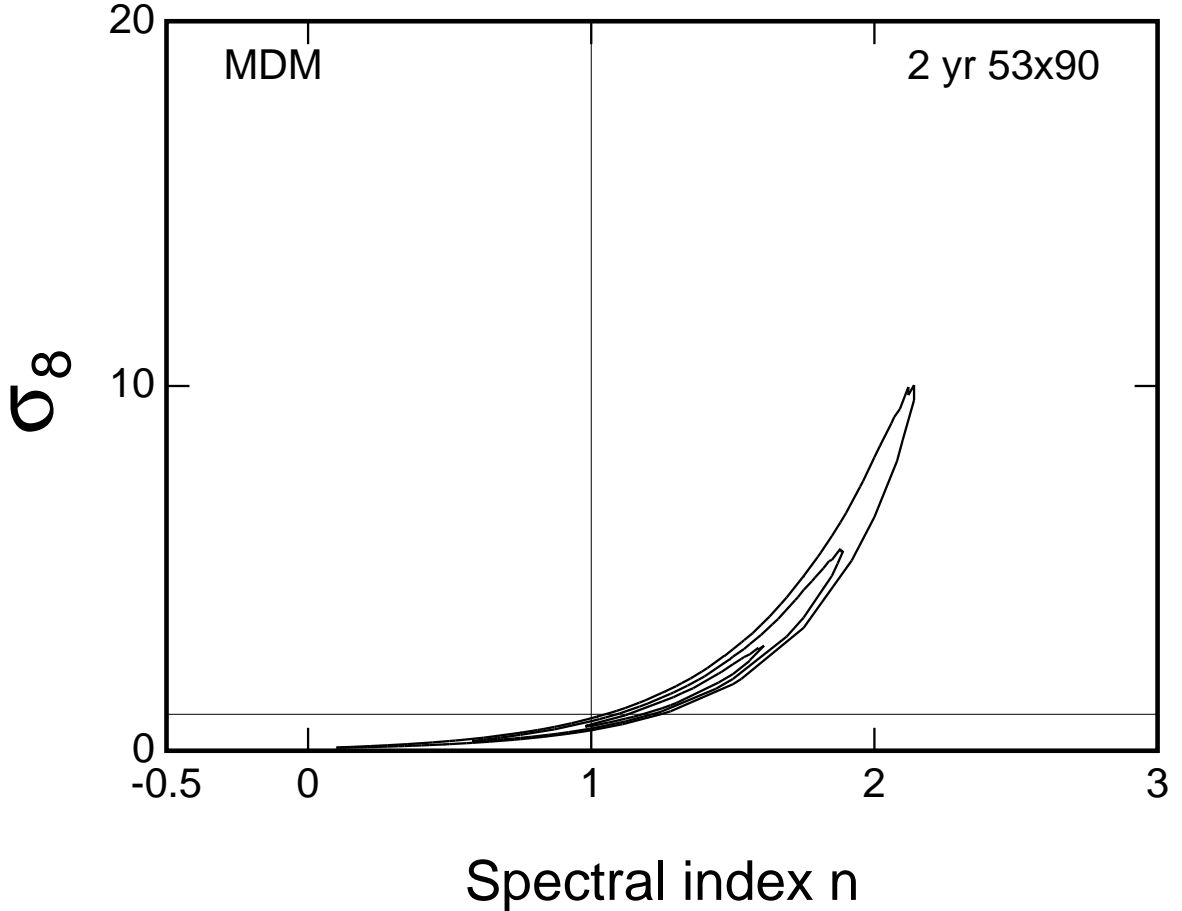


Fig. 2.— Likelihood contours vs σ_8 and n , based on the 2 year 53×90 cross power spectrum for $3 \leq \ell \leq 30$.

where p_p is the prior density. In this case it is true that

$$p_a(n) = \int p_a(Q, n) dQ \propto \int p_p(Q, n) L(Q, n) dQ. \quad (3)$$

Assuming a “uniform” prior to represent prior ignorance then gives the form in Equation 2. But a uniform prior in Q^2 is not the same as a uniform prior in $\ln Q$, and they give different values of n . Different ways of expressing our prior ignorance should not affect the answer. A more dramatic example is shown in Figure 1 and Figure 2, each showing the likelihood contours for the Hauser-Peebles cross power spectrum of the 53×90 2 year maps. In one case they are plotted versus $Q^2 = T_2^2$, while in the other case they are plotted versus the relative mass fluctuations in $8h^{-1}$ Mpc spheres, $\sigma_8 \propto T_{\approx 650}$. The Jacobian of the transformation between (Q^2, n) and (T_{650}, n) depends on n , so a uniform prior in (Q^2, n) becomes an n -dependent prior in (T_{650}, n) . Hence the $\int L(Q, n) dQ^2$ peaks at a much lower n than the $\int L(Q[\sigma_8, n], n) d\sigma_8$.

There is a better way, which is to use the maximum of $L(Q, n)$ for a fixed n to

generate the marginal likelihood over n . This approach to “uninteresting” parameters is recommended by Avni (1976). The maximum value does not require a Jacobian when transforming to different amplitude variables, so prior ignorance of Q^2 gives the same answer as prior ignorance of T_{650} .

The process of determining an amplitude parameter (usually $\langle Q_{RMS}^2 \rangle^{0.5}$) and the spectral index n from the *COBE* maps is an extreme example of data *reduction*. In this process one takes the 360×10^6 DMR data samples per year and produces maps with 6×6144 values, and from these maps one calculates a smaller number of statistics. In the final step, $\langle Q_{RMS}^2 \rangle^{0.5}$ and n are estimated using the values of the statistics, leaving only 2 values derived from nearly 10^9 input values. This description is general enough to describe both the Górski (1994) method using linear statistics and the methods involving quadratic statistics: the correlation function used by Bennett *et al.* (1994) and the Hauser-Peebles power spectrum used by Wright *et al.* (1994). The final result of any of these analysis methods is the values Q_{obs} and n_{obs} determined from the real data, as well as an estimate $\hat{\sigma}_1$ for the noise standard deviation in one observation.

3. Monte Carlo Simulations

In order to test these methods for biases, it is necessary to simulate both the *cosmic variance*, which gives a random map with random spherical harmonic amplitudes chosen from a Gaussian distribution with a variance determined from the chosen Q_{in} and n_{in} , and the *experimental variance*, which gives the 360 million noise values needed per year. While programs to simulate the DMR time-ordered data do exist, none of the groups mentioned above have worked at this level of detail. Instead, they have used simulations that start with the maps.

The effect of noise on the map production process can be simulated using

$$T = \sigma_1 A^{-0.5} U \tag{4}$$

where σ_1 is the noise in one observation, U is an uncorrelated vector of unit variance zero mean Gaussian random variables, and A is the matrix with diagonal elements A_{ii} equal to the number of times the i^{th} pixel was observed, and off-diagonal elements $-A_{ij}$ equal to the number of times the i^{th} pixel was referenced to the j^{th} pixel. Even though A is singular, Wright *et al.* (1994) give a rapidly convergent series technique for generating noise maps. Thus each noise map depends on 6144 independent Gaussian unit variance random variables and the parameter σ_1 .

The signal map that is added to the noise maps to give the “observed” maps is generated using independent Gaussian random amplitudes. Bond & Efstathiou (1987) show that the expected variance of the coefficients $a_{\ell m}$ in a spherical harmonic

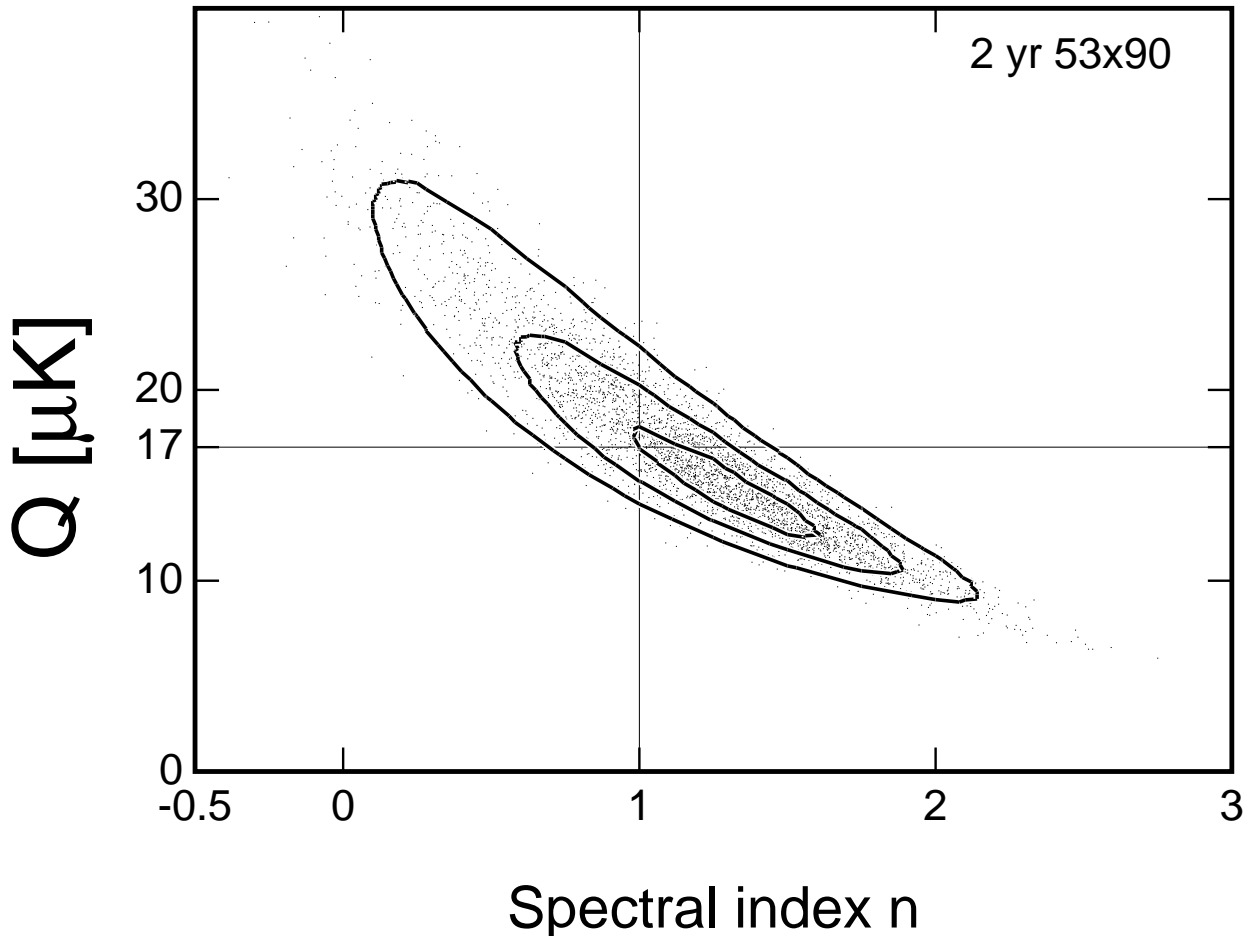


Fig. 3.— Each point is an input parameter set that is consistent with the real data for a given realization of the random cosmic and radiometer variance processes. The likelihood contours are at $\Delta(-2 \ln L) = 1, 4$ and 9 .

expansion of the CMBR temperature given a power law power spectrum $P(k) \propto k^n$ is $\langle a_{\ell m}^2 \rangle \propto \Gamma[\ell + (n - 1)/2] / \Gamma[\ell + (5 - n)/2]$ for $\ell < 40$, with the constant of proportionality chosen so that $5 < a_{2m}^2 \rangle / 4\pi = Q^2$. The simulations done by Wright *et al.* (1994) included ℓ 's up to 39, so the signal map depends on 1600 Gaussian independent unit variance random variables and the two parameters Q and n , which I shall call Q_{in} and n_{in} below to distinguish them from the fitted values.

The resulting Monte Carlo map depends on a set of random variables $\{Z\}$ (1600 + 6144 elements for a one map analysis, or 1600 + 12288 for a cross-analysis needing two maps) with a known distribution, and the three parameters Q_{in} , n_{in} and σ_1 . σ_1 can be determined with great precision using the time-ordered data. Hence one needs to run many Monte Carlo simulations with different values of Q_{in} and n_{in} and compare the fitted values Q_{out} and n_{out} to the fitted values for the real data, Q_{obs} and n_{obs} . For any given

realization of $\{Z\}$, the fitted values Q_{out} and n_{out} are a continuous function of the input parameters Q_{in} and n_{in} , and one can choose values $Q_{in} = Q_{match}$ and $n_{in} = n_{match}$ such that $Q_{out} = Q_{obs}$ and $n_{out} = n_{obs}$. By choosing many different realizations of $\{Z\}$, one creates many different Q_{match}, n_{match} pairs. The density of the points in the Q_{match}, n_{match} plane defines a probability density function for the true parameters Q_{true}, n_{true} that does not depend on any prior knowledge but does depend on the experimental result in a reasonable way. The random element in the process comes from $\{Z\}$, whose properties are known. Figure 3 shows this cloud of points for the 2 year 53×90 cross-power spectrum. The bias ($\Delta n = 0.1$) in the Gaussian approximation maximum likelihood method applied to the quadratic power spectrum statistics is only 0.25σ , so the shift between the points and the contours is hard to see.

The method using linear statistics (Górski 1994) has the advantage that the Gaussian expression for the likelihood is exact. A further advantage of this method is that any non-singular linear transformation of the basis functions will give the same answer, since the covariance matrix will change to cancel the change in the values of the statistics. While this means that the original motivation for generating a set of basis functions orthonormal in the cut sky is lost, one still has the advantage that basis functions orthogonal to any number of low order multipoles are easy to find. Górski *et al.* (1994) find (for $3 \leq \ell \leq 30$) that the maximum of $L(Q, n)$ occurs at $n = 1.02$ for the combined 2 year 53 GHz plus 90 GHz map, and Monte Carlo simulations show that the bias in this application of the maximum likelihood method is small.

Note that the $3 \leq \ell \leq 30$ cross power spectrum fits in Wright *et al.* (1994) still include the off-diagonal effect of the quadrupole on higher ℓ 's, while those in Górski *et al.* (1994) are completely independent of the quadrupole. The modified Hauser-Peebles method in Wright *et al.* (1994) uses basis function defined using

$$G_{\ell m} = F_{\ell m} - \frac{F_{00} \langle F_{00} F_{\ell m} \rangle}{\langle F_{00} F_{00} \rangle} - \sum_{m'=-1}^1 \frac{F_{1m'} \langle F_{1m'} F_{\ell m} \rangle}{\langle F_{1m'} F_{1m'} \rangle}. \quad (5)$$

where the $F_{\ell m}$ are real spherical harmonics and the inner product $\langle fg \rangle$ is defined over the cut sphere. These functions $G_{\ell m}$ are orthogonal to monopole and dipole terms on the cut sphere. Call this the MD method since the basis functions are orthogonal to the monopole and dipole. Let the MDQ method use basis functions orthogonal to the monopole, dipole and quadrupole:

$$G'_{\ell m} = F_{\ell m} - \frac{F_{00} \langle F_{00} F_{\ell m} \rangle}{\langle F_{00} F_{00} \rangle} - \sum_{m'=-1}^1 \frac{F_{1m'} \langle F_{1m'} F_{\ell m} \rangle}{\langle F_{1m'} F_{1m'} \rangle} - \sum_{m'=-2}^2 \frac{F_{2m'} \langle F_{2m'} F_{\ell m} \rangle}{\langle F_{2m'} F_{2m'} \rangle}. \quad (6)$$

Changing from the MD method to the MDQ method causes the mean power in T_4^2 for $n = 1$ Monte Carlo skies to go down by 31% while T_4^2 for the real sky goes up by 16%. This leads to a higher $\ell = 4$ point and a lower value of n ($n = 1.02$ instead of 1.22 for the 53×90 cross-power spectrum). Figure 4 shows the hexadecapole power in μK^2 measured two different ways: on the x axis the MD method; and on the y axis T_4^2 measured using

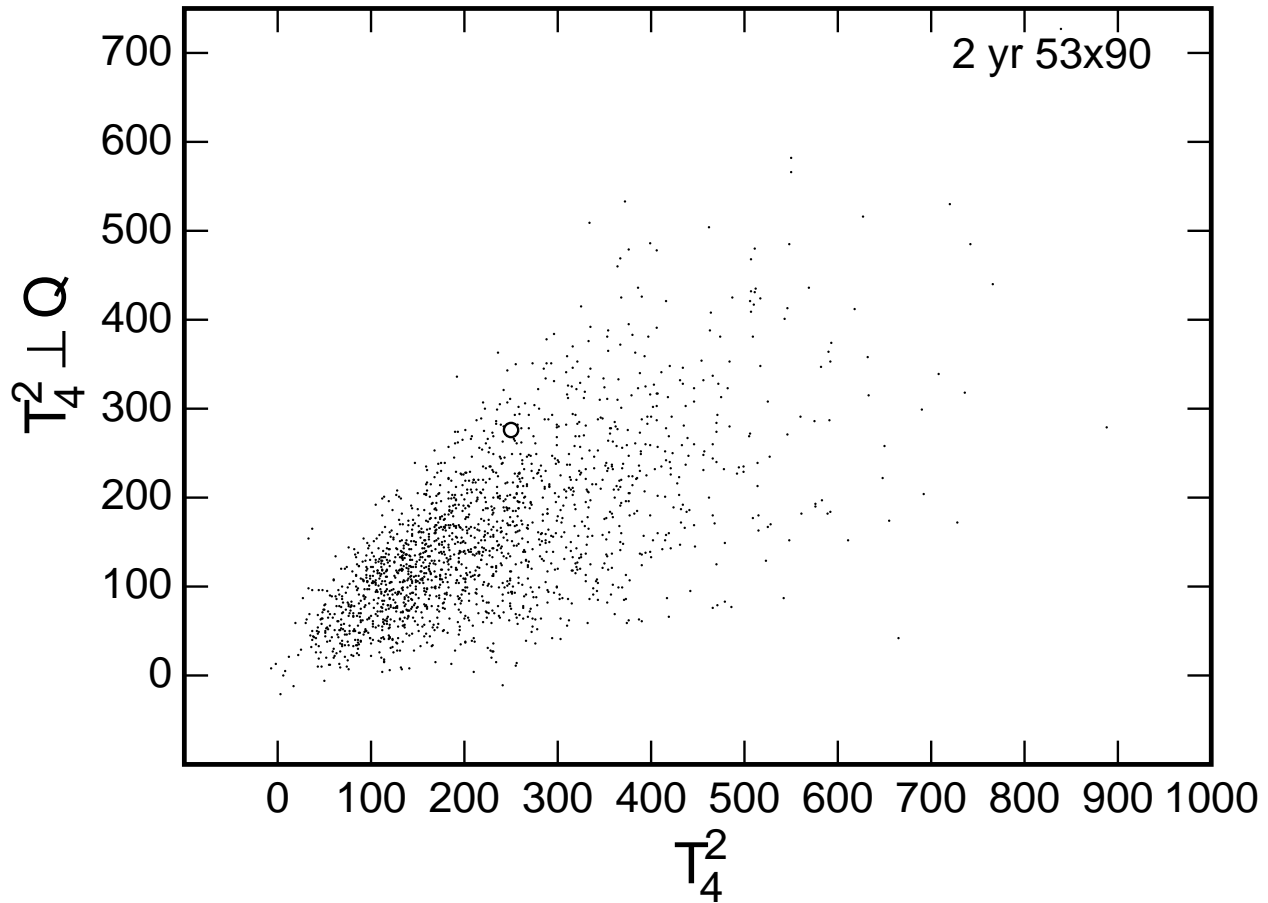


Fig. 4.— Hexadecapole power determined using the MD method on the x -axis *vs.* the MDQ method on the y -axis for the real sky (open circle) and $n = 1$, $\langle Q_{RMS}^2 \rangle^{0.5} = 17 \mu\text{K}$ simulations.

the MDQ method. The real sky is shown as the open circle, while the dots are $n = 1$, $\langle Q_{RMS}^2 \rangle^{0.5} = 17 \mu\text{K}$ Monte Carlo simulations. One sees that the real sky is moderately far out on the upper edge of the cloud of simulations, and this produces the 0.5σ shift in n when changing basis functions. One also sees that the distribution of T_4^2 is quite skewed, which explains the bias in the method that maximizes the Gaussian approximation to the likelihood.

Figure 5 shows the maximum likelihood values of n from fits to $3 \leq \ell \leq 30$ for 1800 Monte Carlo runs with $n_{in} = 1$ and $Q_{in} = 17 \mu\text{K}$. The x -axis shows n computed using the MD method, while the y -axis shows the results of the MDQ method. The real sky is shown as the open circle, and the mean of the 1800 Monte Carlo spectra is shown as the closed circle. This figure shows that the two methods are generally consistent, with the real sky moderately far out in the scatter. (The linear features for $n = 1.00$, 1.25 and 1.50 are caused by the interpolation among input values spaced by $\Delta n_{in} = 0.25$ during the maximum likelihood fits.) The overall performance of the MD method is better, with a bias

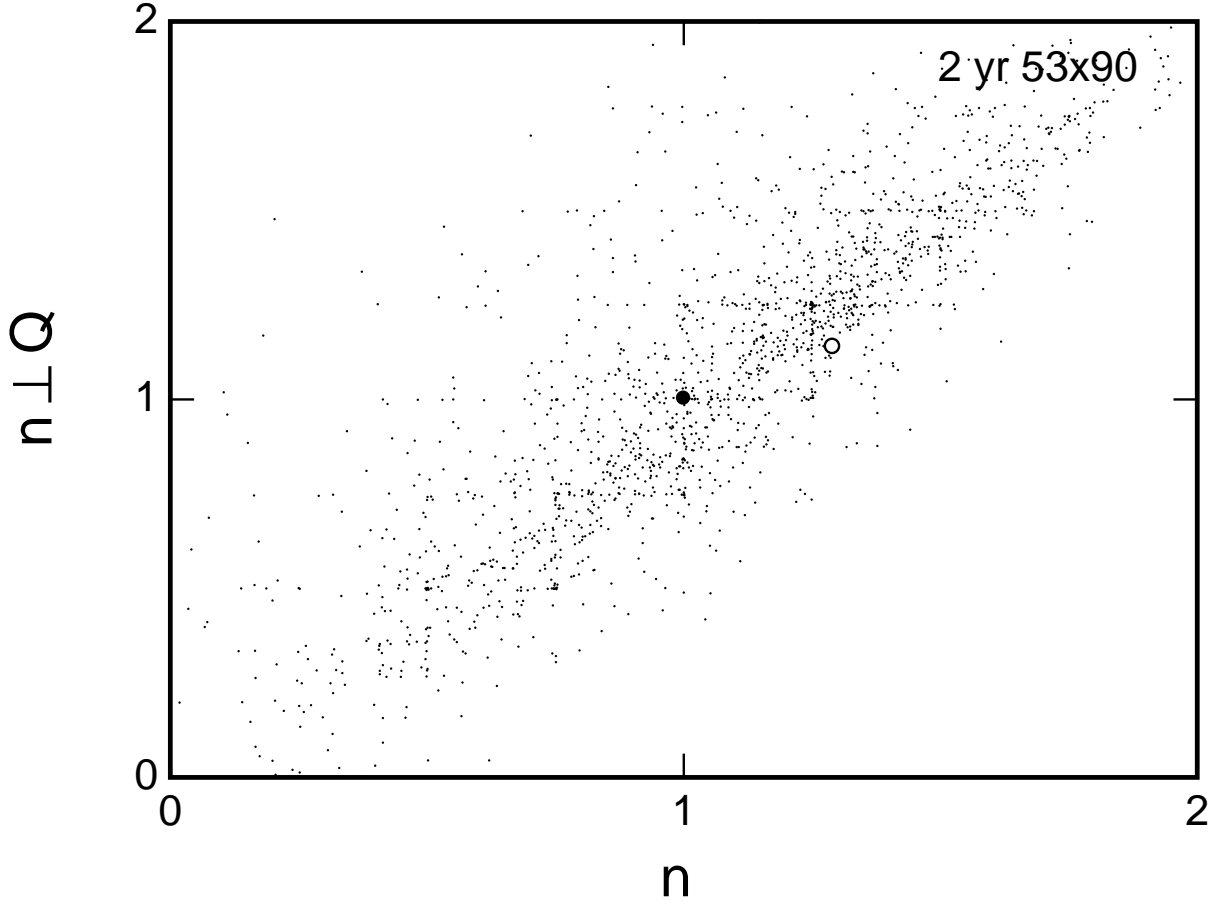


Fig. 5.— Spectral index n using the MD method on the x -axis *vs.* n from the MDQ method for 1800 Monte Carlo skies with $n_{in} = 1$ and $Q_{in} = 17 \mu\text{K}$. The real sky is the open circle.

that is 20% smaller and a standard deviation that is 8% smaller than those given by the MDQ method. Of course fits that include the quadrupole ($2 \leq \ell \leq 30$) do even better, since they use more information. So the final result of the power spectral analysis is ambiguous: $n \approx 1.4$ if the quadrupole is included in the fit, $n \approx 1.25$ excluding the quadrupole using the MD method, or $n \approx 1.0$ when rigorously excluding the quadrupole using the MDQ method. The existence of all these options raises the specter of “optional stopping”, a time-honored method of introducing systematic errors into measurements. But fortunately this whole range of values is within the statistical uncertainty.

Even in very simple cases this level of disagreement between different estimation techniques is common. For example, the RMS difference between the median and the mean of a set of Gaussian random numbers is $3/4$ of the standard deviation of the mean.

4. Degree-Scale

The experiments at $\approx 1^\circ$ scale offer the possibility of a better determination of the primordial power spectrum index n , but the model-dependent effects of the wing of the Doppler peak at $\ell \approx 200$ must be allowed for. Even in the large angle region $\ell < 30$ small model-dependent corrections must be made. A Cold Dark Matter (CDM) model with a primordial spectral index $n_{pri} = 0.96$ has an apparent index $n_{app} = 1.1$ due to the “toe” of the Doppler peak that extends into the $\ell < 70$ region. Wright *et al.* (1994) have made this comparison with degree scale experiments, and the resulting value for n_{pri} is given in Table 1.

5. Large Scale Structure

A comparison of the extremely large scale structure seen by *COBE* to the large scale structure seen in studies of the clustering of galaxies also leads to an estimate of n_{pri} . The uncertainty in this method is decreased because of the large range of scales covered, but also increased due to uncertainties in the models of large scale structure formation. However, this comparison strongly favors $n = 1$. Prior to the *COBE* announcement of anisotropy, Peacock (1991) gave an implicit prediction that for $n = 1$ the amplitude of ΔT should be $\langle Q_{RMS}^2 \rangle^{0.5} = 18.8 \mu\text{K}$. Peacock & Dodds (1994) have extended this analysis of large scale structure and I get a result $n_{pri} = 0.99 \pm 0.16$ from their paper after correcting for their incorrect $\langle Q_{RMS}^2 \rangle^{0.5} = 15 \mu\text{K}$ and increasing the uncertainty to allow for the uncertainty in the IRAS bias, b_I . In Figure 6 I have “extended” Figure 6 from Peacock & Dodds to include the *COBE* datum, and show extrapolations with $n = 0.5, 1, \& 1.5$ through the *COBE* point. This result assumes that $\Omega = 1$, but Peacock & Dodds have also found that $\Omega^{0.6}/b_I = 1.0 \pm 0.2$.

6. Summary

In conclusion, both the *COBE* ΔT data alone and the ratio of the *COBE* ΔT data to 1° scale ΔT are consistent with the $n \approx 1$ prediction of the inflationary scenario. Furthermore, the implied level of gravitational potential perturbations is sufficient to produce the observed large scale (100 Mpc) structure if both the $n = 1$ and $\Omega = 1$ predictions of inflation are correct, and the Universe is dominated by Dark Matter.

| Method | COBE dataset | Q? | Result | Reference |
|----------------------------|----------------|----|----------------------------------|---------------------------|
| Correlation function | 1 year 53×90 | N | $n_{app} = 1.15^{+0.45}_{-0.65}$ | Smoot <i>etal</i> ('92) |
| COBE: σ_8 | 1 year 53+90 | N | $n_{pri} = 1 \pm 0.23$ | Wright <i>etal</i> ('92) |
| Genus <i>vs.</i> smoothing | 1 year 53 | Y | $n_{app} = 1.7^{+1.3}_{-1.1}$ | Smoot <i>etal</i> ('94) |
| RMS <i>vs.</i> smoothing | 1 year 53 | Y | $n_{app} = 1.7^{+0.3}_{-0.6}$ | Smoot <i>etal</i> ('94) |
| Correlation function | 2 year 53×90 | Y | $n_{app} = 1.3^{+0.49}_{-0.55}$ | Bennett <i>etal</i> ('94) |
| Correlation function | 2 year 53×90 | N | $n_{app} = 1.1^{+0.60}_{-0.55}$ | Bennett <i>etal</i> ('94) |
| COBE: 1° scale | 2 year NG | N | $n_{pri} = 1.15 \pm 0.2$ | Wright <i>etal</i> ('94) |
| Cross power spectrum | 2 year 53 & 90 | N | $n_{app} = 1.25^{+0.40}_{-0.45}$ | Wright <i>etal</i> ('94) |
| Cross power spectrum | 2 year 53 & 90 | Y | $n_{app} = 1.39^{+0.34}_{-0.39}$ | |
| Orthonormal functions | 2 year 53+90 | N | $n_{app} = 1.02 \pm 0.4$ | Górski <i>etal</i> ('94) |
| COBE: σ_{100} | 1 year 53 | Y | $n_{pri} = 1.0 \pm 0.16$ | Peacock & Dodds |

Table 1: Spectral index determinations

7. References

Avni, Y. 1976, ApJ, 210, 642-646.

Bennett, C. L., Kogut, A., Hinshaw, G., Banday, A. J., Wright, E. L., Gorski, K. M., Wilkinson, D. T., Weiss, R., Smoot, G. F., Meyer, S. S., Mather, J. C., Lubin, P., Lowenstein, K., Lineweaver, C., Keegstra, P., Kaita, E., Jackson, P. D. & Cheng, E. S. 1994, ApJ, TBD, TBD.

Bond, J. R. & Efstathiou, G. 1987, M.N.R.A.S, 226, 655-687.

Górski, K. M. 1994, submitted to the ApJL.

Górski, K. M., Hinshaw, G., Banday, A. J., Bennett, C. L., Wright, E. L., Kogut, A., Smoot, G. F. & Lubin, P. 1994, submitted to the ApJL.

Hauser, M. G. & Peebles, P. J. E. 1973, ApJ, 185, 757-785.

Peacock, J. A. 1991, MNRAS, 253, 1p-5p.

Peacock, J. A. & Dodds, S. J. 1994, MNRAS, 267, 1020-1034.

Smoot, G. F. *etal.* 1992, ApJL, 396, L1.

Smoot, G. *et al.* 1994, submitted to the ApJ

Wright, E. L., Smoot, G. F., Bennett, C. L. & Lubin, P. M. 1994, ApJ, TBD, TBD.

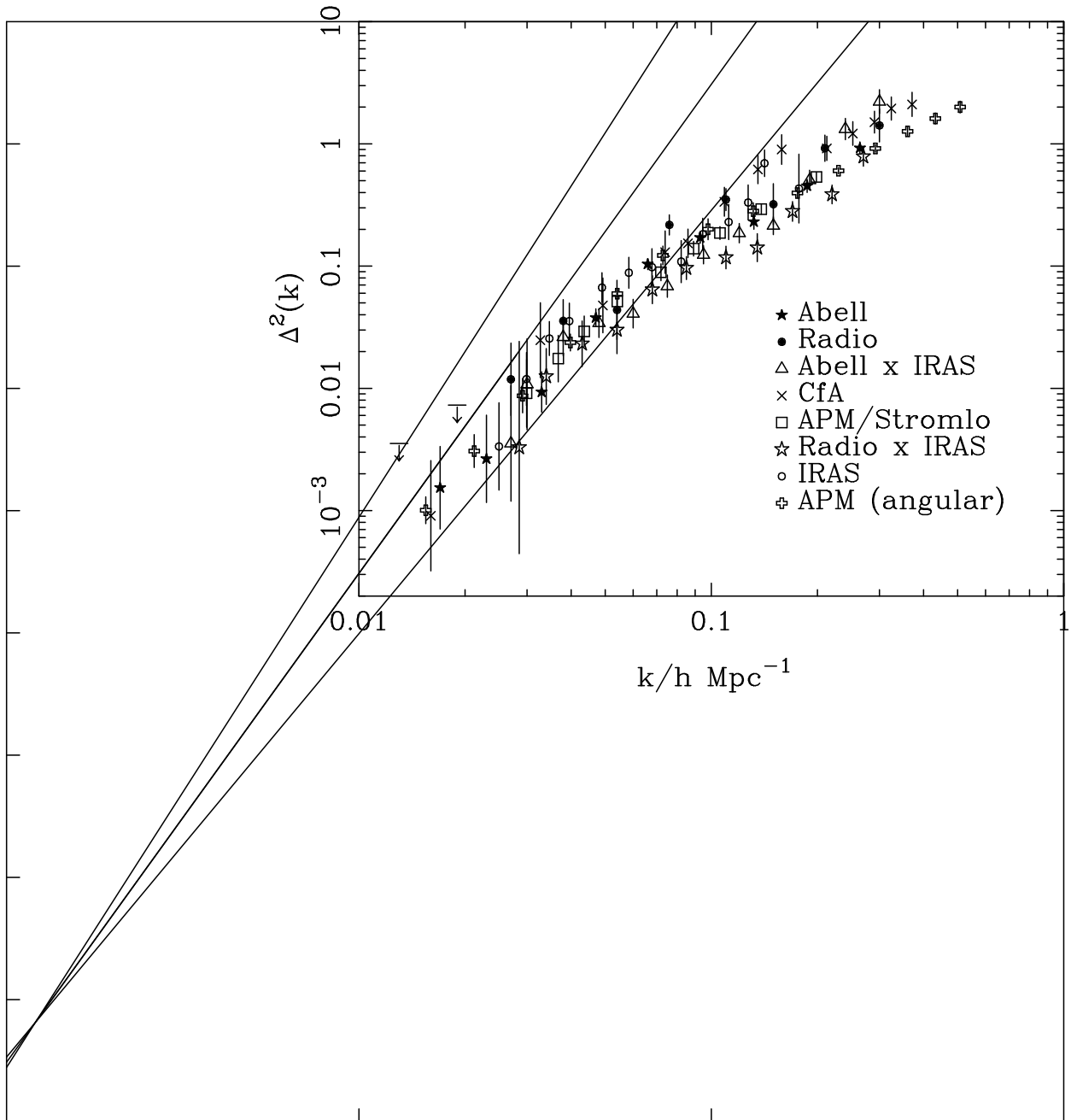


Fig. 6.— An extended version of Figure 6 from Peacock & Dodds, showing $n = 0.5, 1$ and 1.5 extrapolations through the *COBE* point.